Characterization and Adsorption Applications of Composite Biochars of Clay Minerals and Biomass

Lihui Gao (lihuigaocumt@163.com)
China University of Mining and Technology
Jillian L. Goldfarb
Cornell University

Research Article

Keywords: Composite biochar, clay minerals, pyrolysis, adsorption, multilinear model

Posted Date: March 16th, 2021

DOI: https://doi.org/10.21203/rs.3.rs-295822/v1

Version of Record: A version of this preprint was published at Environmental Science and Pollution Research on April 13th, 2021. See the published version at https://doi.org/10.1007/s11356-021-13858-x.

Characterization and adsorption applications of composite biochars of clay minerals and biomass

Lihui Gao[1*] and Jillian L. Goldfarb[2]

1. School of Environment and Spatial Informatics, China University of Mining and Technology, Xuzhou 221116, People's Republic of China

2. Department of Biological and Environmental Engineering, Cornell University, 226 Riley-Robb Hall, Ithaca, NY 14853, USA

Abstract: Composite mineral-biochars of a homogeneous biomass (cellulose) and heterogeneous biomass (oak leaves) were fabricated with either 5*wt*% or 10*wt*% minerals (montmorillonite (MMT), kaolinite, and sand), and then pyrolyzed at 600 °C for 60 min. Characterizations including proximate analysis, ultimate analysis, surface area and porosity, morphology and surface chemistry confirmed that minerals were present on the surface of biochar, and MMT/kaolinite-biochar composites showed a strengthening in the chars' aromatic structures, as well as increases in oxygen-containing surface functional groups. Methylene blue adsorption isotherms indicated that the MMT/kaolinite-biochars had higher adsorption capacities than pure biomass or biomass-sand biochars (110 mg_{MB}/g_{char} and 24 mg_{MB}/g_{char} for MMT-cellulose char and cellulose char, respectively). A multilinear model relating adsorption capacity and adsorbent properties was developed to measure the relative contribution of biochar properties to adsorption behavior. The model indicates that pore volume and hydrogen

* To whom correspondence should be addressed (lihuigaocumt@163.com)

bonding were the dominant properties in controlling the adsorption of methylene blue onto the biochars. Findings from this work indicate that composite biochars prepared from biomass and inexpensive clay minerals are a promising adsorbent for remediating organic contaminants from water.

Keywords: Composite biochar; clay minerals; pyrolysis; adsorption; multilinear model

1. Introduction

Biochar, a carbonaceous solid resulting from biomass pyrolysis under inert conditions, has gained much attention because of its promising application as a soil amendment, or, upon upgrading into activated carbons, as fuel cell and supercapacitor electrodes, gas adsorbents, and for water treatment to remove a variety of organic and inorganic contaminants(Dehkhoda et al., 2016a, 2016b; Kimetu et al., 2014; Tan et al., 2017, 2015; Wu et al., 2017). Multiple methods (e.g. chemical and physical activation techniques(Istan et al., 2016; Tay et al., 2009; Vijayalakshmi et al., 2010)) have been developed to modify biochar and increase its adsorption capacity for various pollutants in the aqueous environment.

Due to their unique layered structure, high specific surface area and ion exchange capacity, clay minerals show great potential in agriculture as well as in industrial and petroleum engineering(Murray, 1991). Among them, montmorillonite and kaolinite are perhaps the most studied clays across various research areas. Montmorillonite (MMT) is a 2:1 layered aluminosilicate, and there are exchangeable cations (Na^+, K^+, Ca^{2+}, etc.) with strong electron-acquiring ability and adsorption performance between the layers. One important characteristic of MMT is that the layers are negative charged, and the charge is usually balanced by hydrated cations located within the interlayer space(Segad et al., 2010). Kaolinite is a 1:1 layered aluminosilicate; the internal charge is close to balanced, and there are no exchangeable cations or water molecules between the layers(Chcn et al., 1999). Thus, the exchange sites of kaolinite are only located on the surface. Yet, both clays have been shown – in raw and modified forms – to be

effective adsorbent materials for a range of environmental contaminants. For example, Sherbini and Hassanien(Abou-El-Sherbini and Hassanien, 2010) used 2-Oxyhydrazino-N-(2-methylen-yl-hydroxyphenyl)pyridinium (OMHP) ion to modify MMT to remove Cu(II), results showed that OMHP-MMT had a good removal efficiency and selectivity towards Cu(II) with a removal capacity of 119 mEq/100g. Jiang *et al*.(Jiang et al., 2010) used kaolinite clay to adsorb heavy metal ions from wastewater; their results showed that the adsorption capacity of kaolinite for Pb^{2+} reached 160 mg/L under the synergistic mechanisms of adsorption and ion exchange. However, MMT and kaolinite may not be suitable as fixed-bed media or additives in water treatment due to their fine particle size (i.e., colloids/nanoparticles).

Engineering methods have been widely applied to create biochar-based materials with upgraded functionalities for environmental applications. In such biochar-based composites, biochar provides a porous structure that can support clay micro- and nanoparticles within the carbonaceous matrix. Therefore, a simple method was developed to synthesize mineral-biochar material for environmental applications. In order to investigate the upgraded performance of clay minerals on different biomass substrates, two different biomasses (“homogeneous” biomass, microcrystalline cellulose; a “heterogeneous” biomass, dried oak leaves) were selected and each was mixed well with one of the clay minerals prior to pyrolysis. The physicochemical properties of these pyrolyzed chars were characterized. In addition, the adsorption property of engineering bio-chars to methylene blue (MB), which is regarded as a “model” organic compound for adsorption(Gao and Goldfarb, 2019; Yao et al., 2014),

was measured to evaluate the potential application in environmental remediation. Therefore, the objectives of this research are to: (1) prepare mineral-biochar composites; (2) characterize their physiochemical properties; (3) measure the adsorption ability to remove MB; (4) explore the adsorption mechanisms of MB adsorb onto the composites.

2 Material and Methods

2.1 Biochar fabrication

Cellulose (Alfa Aesar) was supplied by Fisher Scientific. Oak leaves were collected in Boston, MA in late October / early November 2016 from a representative set of trees. To remove dust, leaves were washed in deionized water and dried in a laboratory oven to prevent degradation. The leaves were ground and sieved to a particle size fraction of 100 to 300 μm. Raw biomasses were blended with sand (Sigma-Aldrich), kaolinite (Fisher scientific,), or montmorillonite clay (Sigma-Aldrich), at 5 *wt*% and 10 *wt*% mineral loadings. Samples were weighed directly into a glass vial to the 0.1 mg, and homogenized on a vortex mixer. The characteristics of the biomass feedstock and three types of minerals were showed in Table S1-2 and Figure S1-3 in supplemental information.

Biochar was fabricated by pyrolyzing between 1.5 and 2 g of raw biomass or biomass-mineral blend in a 2" MTI tube furnace. A large number of studies have shown that the biochar-based composites synthesized via pyrolysis at 600°C has a highly efficient sorption performance(Zhang et al., 2013; Zhang and Gao, 2013). Therefore, this paper sets the final pyrolysis temperature as 600°C , and the detailed pyrolysis parameters are as follows: To ensure an inert atmosphere, the furnace was purged with

nitrogen for 5 minutes, and then heated at 5 °C/min to 110 °C and held for 30 minutes, and then to 600 °C at 5 °C/min and held for 60 min under constant nitrogen flow of approximately 115 mL/min. Samples were cooled in a nitrogen atmosphere to prevent oxidation.

Raw samples were named as: RL (Raw Oak Leaves) and RC (Raw cellulose). Pyrolyzed biochars were named as PL (Pyrolyzed leaves); PLK (Pyrolyzed Leaves + Kaolinite); PLM (Pyrolyzed Leaves + Montmorillonite); PLS (Pyrolyzed Leaves + Sand); PC (Pyrolyzed Cellulose); PCK (Pyrolyzed Cellulose + Kaolinite); PCM (Pyrolyzed Cellulose + Montmorillonite); PCS (Pyrolyzed Cellulose + Sand) followed by the mass fraction of clay minerals, e.g. LK5, LK10, CM5, CM10, etc.

2.2 Biochar characterization

A Mettler-Toledo TGA-DSC-1 thermogravimetric analyzer–differential scanning calorimeter was used to determine proximate analysis of biomass and biochar. Briefly, samples were loaded into 70 μL alumina crucibles. Samples were heated from room temperature to 110°C under 20 mL/min N_2 gas and held for 30 minutes to remove moisture. Samples were then heated at 10°C/min to 900°C and held for 60 minutes (loss attributed to volatile matter), and then the gas was switched to dry air and sample heated to 950°C, held for 60 minutes (loss attributed to fixed carbon, residual loosely termed "ash.") The ultimate analysis on the raw biomass and biochar was conducted using a CHNS Elemental Analyzer (Vario Macro Cube, Germany).

Nitrogen adsorption isotherms, performed on a Quantachrome Autosorb-iQ, were used to measure the surface areas and porosities of the biochars. Samples were degassed

at 180 °C for a minimum of 12 h (with the exception of the raw biomass, which was degassed at 80°C to prevent pyrolysis), and then weighed on a Sartorius semi-microbalance to ±0.1 mg. The Brunauer-Emmett-Teller (BET) adsorption method was employed over a partial pressure range of 0.05–0.3 in ultra high purity nitrogen at liquid nitrogen temperature(Brunauer et al., 1938). Scanning electron microscope (SEM) imaging of the biochar samples was conducted on a Zeiss Supra 55VP field emission scanning electron microscope. FTIR spectra were recorded between 4000 and 400 cm^{-1} on a Nicolet 380 Thermo Scientific spectrometer. Cation exchange capacity (CEC) was obtained using the ammonium acetate method in which 0.02 g of the biochar/clay was added to 5 mL of 0.5 M ammonium acetate solution. The mixture was agitated for 6 h, filtered, and the filtrate kept for inductively coupled plasma-mass spectrum (ICP-MS) analysis of Na^+, K^+, Ca^{2+}, and Mg^{2+}. The exchangeable cations were determined via:

$$\text{Exch. Ca} = \frac{C_0 \times 5}{10 \times 20.04 \times m_0} - \frac{C_1 \times 5}{10 \times 20.04 \times m_1}$$

$$\text{Exch. Mg} = \frac{C_0 \times 5}{10 \times 12.15 \times m_0} - \frac{C_1 \times 5}{10 \times 12.15 \times m_1}$$

$$\text{Exch. K} = \frac{C_0 \times 5}{10 \times 39.1 \times m_0} - \frac{C_1 \times 5}{10 \times 39.1 \times \mathrm{m}_1}$$

$$\text{Exch. Na} = \frac{C_0 \times 5}{10 \times 23.0 \times m_0} - \frac{C_1 \times 5}{10 \times 23.0 \times m_1}$$

Where C_0=concentration of Ca, Mg, K, and Na (mg/L) from the extract solution; C_1=concentration in blank solution; m_0=weigh of biochar/clay (g) in ammonium acetate solution m_1=weigh of biochar/clay (g) in ultrapure water; and 5 = volume of NH_4OAc used in mL. 40.078, 24.305, 39.098, 22.99 are the atomic weights of Ca, Mg, K, and Na, respectively, in g/mol. The cation exchange capacity is the summation of Ca^{2+},

Mg^{2+}, Na^{+}, and K^{+} exchangeable cations.

2.3 Application of biochar to water treatment

To determine the effect of different clay minerals on resulting biochars' adsorption potential, we used the pure biomass-char and 5 *wt*% mineral loaded biochars in standard methylene blue (MB) adsorption kinetics and isotherm experiments(Visa et al., 2010). Batch adsorption isotherm experiments were run in 5 mL glass vials with a 1:500 ratio (0.008 g biochar in 4 mL solution) using MB solutions having initial concentrations from 20 to 200 mg/L at room temperature.

Kinetic adsorption experiments were carried out using a 50 mL flask at room temperature with a 1:500 (0.08 g biochar in 40 mL solution). 100 mg/L MB solution was used, and samples were collected at time intervals of 5, 10, 20, 30 min, and 1, 2, 4, 6, 8, 24, 48 h. The samples were shaken on a shaker table at 100 rpm, and samples were withdraw using a pipette, and immediately filtered through 0.45 μm pore size hydrophilic PVDF membrane filters.

Dye concentrations for both experiments were determined on a Shimadzu UV-vis 1800 spectrophotometer at 664 nm.

3 Results and discussion

To test the hypothesis that clay minerals, known for their adsorptive properties, could enhance the adsorption capacity of biochars when co-pyrolyzed at relatively low loadings (5 and 10 wt%), we fabricated a series of 14 biochars and characterized their resulting properties and adsorption capacities.

3.1 Characterization of biochars

As noted in Table 1, the pure biomass chars (PL and PC) show higher volatile matter, fixed carbon and elemental C content versus the mineral-biochar composites. This is mainly because of the increased relative concentration of minerals. The carbon content of cellulose-based biochars was higher than that of the oak leaves-based biochars, indicating that raw biomass type more strongly influences the biochar's carbon level, rather than the specific mineral with which the biomass is mixed. Yao *et al.*(Yao et al., 2014) and Basta *et al.*(Basta et al., 2011, 2009) also suggested that the chemical constituents of raw material (the ratios of cellulose, lignin, and hemicellulose in a heterogeneous biomass) control the yield and quality of biochar. The nitrogen and sulphur contents of all the sample were comparable with each other and ranged from 0.5~0.8%/0.03~0.06% and 0.2~0.4%/0.51~0.67% for leave type/cellulose type. Comparing biochar of the same biomass type and mineral loading, the reported data showed that carbon content of MMT-biochar was the highest. MMT loading resulted in production of biochar with high carbon content; at the same time, stronger catalytic effect of MMT aided the loss of hydrogen as a result of cleavage of weak bonds in biochar. Since the surface and interlayers of MMT contains more Lewis sites and Brønsted sites than kaolinite, the performance of catalyzing hydrocarbon generation during biomass pyrolysis was significantly higher than that of other mineral(Luo et al., 2021; Yang et al., 2009). Hence, MMT might promote more organic matter devolatilization and subsequent resulting a biochar with higher carbon content and lower hydrogen content. The calculated atomic ratios of O/C; H/C and (O+N)/C for

MMT-biochar was lower than the same biomass type with same weight clay loading. The reduction of H/C in the biochar is an indication of effective carbonization of the biomass while a decrease in the ratio of O/C is attributed to polarity reduction and the hydrophilicity nature of the biochar surface(Ahmad et al., 2012). The ratio of H/C and O/C were used as an indicator for carbonization and reduction in this ratio indicated that there was a loss of water and O-containing functional groups in the present of MMT catalyst, which converted the alkyl carbon to aromatic carbon(Uchimiya et al., 2011).

3.1.1. Surface Area of Biochars

The surface areas increase 1-2 orders of magnitude upon pyrolysis of the raw biomass. In addition, for leaf-based biochar, the surface area of the mineral-biochar with 5*wt*% loading was 2-4 times higher than PL, yet the surface area of cellulose-mineral biochar was lower than PC. Proximate analysis suggested that mineral loaded chars have lower volatile matter contents because of the mineral-promoted devolatilization during the pyrolysis process (and increase in ash content and some fixed carbon from the minerals); MMT's catalytic performance was higher than that of kaolinite. In general, the pores of the solid biomass expand as the volatile substances escape, generating a biochar with a larger specific surface area than its raw biomass counterpart(Gao and Goldfarb, 2019). Interestingly, the surface areas of MMT-biochars were lower than those of the kaolinite-biochars, and while the surface area of the 5 wt% MMT and kaolinite biochars for the leaves were higher than the unamended biomass, the surface areas of all the mineral-biochar composites showed a decreasing trend with

209 increasing mineral loading. This suggests that the porous voids formed during
210 devolatilization might be blocked by minerals or have collapsed (plausible given the
211 small ratio of volatile matter present), both of which would result in lower surface area
212 and pore volume(Dou and Goldfarb, 2017).

213 **Table 1**. Proximate, ultimate, and surface area analyses results on composite biochars fabricated from minerals and either oak leaves or cellulose

Samples	V_M (%)	FC (%)	Ash (%)	C (%)	H (%)	O (%)	N (%)	S (%)	H/C	O/C	(O+N)/C	S_{BET} (m^2/g)	V_{Total} (cm^3/g)	Pore size (nm)
RL	83.24	12.32	4.44	53.94	5.93	39.32	0.7	0.11	0.11	0.73	0.74	1.29	0.0025	6.903
PL	28.44	58.32	13.24	70.25	2.38	27.37	0.8	0.44	0.03	0.39	0.40	21.61	0.032	2.427
PLK5	23.21	53.47	23.32	62.87	2.14	34.99	0.66	0	0.03	0.56	0.57	92.54	0.083	2.537
PLM5	21.13	59.05	19.82	64.6	2.22	33.18	0.73	0.38	0.03	0.51	0.52	75.16	0.062	2.592
PLS5	23.58	56.66	19.76	64.67	2.41	32.04	0.6	0.28	0.04	0.50	0.50	46.2	0.047	2.462
PLK10	16.63	48.25	35.12	57.44	3.77	37.85	0.57	0.37	0.07	0.66	0.67	91.91	0.078	3.4
PLM10	19.71	49.77	30.52	58.12	3.11	38.11	0.51	0.15	0.05	0.66	0.66	62.67	0.06	3.843
PLS10	23.92	35.05	41.03	54.17	4.68	39.96	0.76	0.43	0.09	0.74	0.75	36.43	0.035	3.849
RC	95.41	4.36	0.23	44.45	6.22	49.34	0	0	0.14	1.11	1.11	1.22	0.0039	13.024
PC	29.82	69.34	0.84	85.28	4	3.43	0	3.43	0.05	0.04	0.04	286.69	0.174	5.853
PCK5	19.51	62.67	17.82	73.5	2.18	24.33	0.03	0.51	0.03	0.33	0.33	284.73	0.181	3.607
PCM5	17.04	64.92	18.04	67.99	2.21	29.8	0.04	0.67	0.03	0.44	0.44	256.16	0.166	3.294
PCS5	28.23	44.56	27.21	67.45	5.83	26.12	0.04	0.56	0.09	0.39	0.39	255.12	0.157	4.068
PCK10	16.45	45.13	38.42	59.83	3.65	35.86	0.05	0.61	0.06	0.60	0.60	250.2	0.164	2.62
PCM10	15.12	55.36	29.52	60.12	3.14	36.04	0.05	0.65	0.05	0.60	0.60	229.78	0.157	2.733
PCS10	16.04	31.02	52.94	58.66	4.24	36.48	0.06	0.56	0.07	0.62	0.62	223.84	0.139	2.481

214

3.1.2 FTIR analysis

The FTIR spectra of the prepared biochars is shown in Figure 1. The surfaces of the two types of clay-based biochars are rich in -OH, -C-O, -COO and -C-H groups. Compared with PC/PL, new bands in MMT-biochar and kaolinite-biochar appeared, including for Si-O (470 cm^{-1}), -C-H (810 cm^{-1}), -C-O/-C=O (1037/1073 cm^{-1}), -COO/-C=C (1571/1580 cm^{-1}) and -OH (3430/3459 cm^{-1}). Given the large increase, especially in oxygen-containing groups (beyond what might be expected by adding 5 or 10 wt% of minerals that contain relatively low oxygen contents), we suspect that the minerals both "add" to the surface character (e.g. through addition of Si-O groups) and interact with the biochar's carbons to enhance the oxygenated groups on the surface of the biochar. This is further seen in the increase in the aromatic -C-H nature (810 cm^{-1})(Goldfarb et al., 2017) upon MMT/kaolinite loading. The presence of one broad band at 1039/1073 cm^{-1}, along with the small peaks at 3430/3459 cm^{-1} indicated the formation of dehydrocarboxyl and -OH, respectively. In addition, the bands around 1580 cm^{-1} corresponding to aromatic C=C, C=O stretching vibration modes of the carboxyl group, hydroxyl group and lactone(Sun et al., 2015) increase with MMT and kaolinite addition (and actually decrease with sand). Therefore, the loading of MMT and kaolinite can strengthen the aromatic structure of pyrolyzed-char, and also increases the oxygen-containing functional groups such as dehydrocarboxyl, carbonyl and hydroxyl groups.

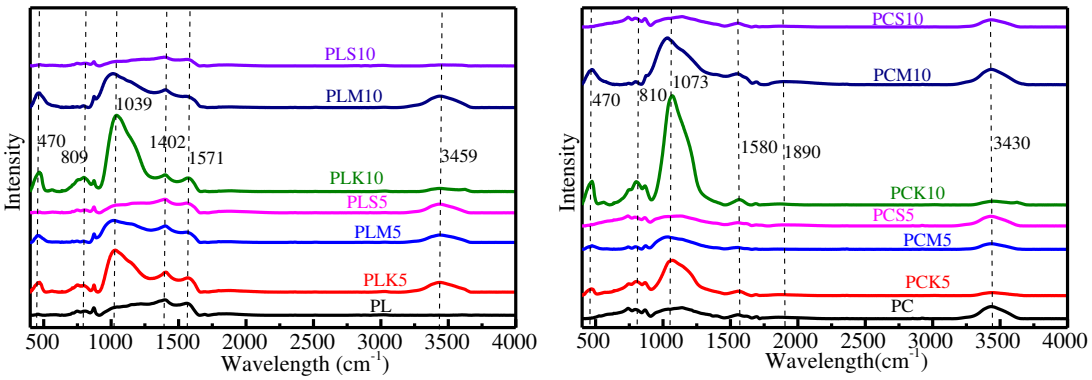

Figure 1. FTIR spectra of prepared biochar

3.1.3 Cation exchange capacity

The CEC is used to describe the potential of a biochar to adsorb positively charged substances. As shown in Figure 2, the CEC values of leaf-based biochars (ranging from 15 to 33 meq/100 g) were higher than cellulose-based biochars (ranging from 1 to 35 meq/100 g). The CEC of oak leaf-biochar and cellulose-biochar was significantly lower than the CEC previously reported for biochar produced from sugar cane bagasse (122 meq/100g) pyrolyzed at 460 °C(Carrier et al., 2012), although similar to the CEC reported for paper mill waste biochar (9-18 meq/100g)(van Zwieten et al., 2010). Suliman *et al*. reported that the CEC was a function of oxygenated functional groups and surface area of biochar(Suliman et al., 2016). However, the surface area of cellulose-based char was much higher than leaf-based char, indicating that surface area of material was likely not the dominant factor controlling CEC. Khawmee *et al*.(Khawmee et al., 2013) and Basak *et al*.(Basak et al., 2020) showed that the CEC of a material was highly correlated with its metal content, oxygenated functional groups, Lewis acid and base sites, which may be consistent with the results of this work.

We can see that the mineral loading had different effects on the various biochars.

The measured CEC value of MMT/sand-leaf biochar or kaolinite/sand-cellulose biochar was quite similar to the predicted value (if we assume that the contribution is a weighted fuction of the composites' constituents as: Predicted CEC=$wt_{Mineral}$*(Mineral CEC)+$wt_{Biomass}$*(PL/PC CEC), where wt is the mass fraction of the component in the blend), indicating the CEC values of these biochar-mineral composites were in an addtive nature way. However, the MMT loaded cellulose biochars (19.34, 35.41 meq/100g) have higher CEC than predicted ones (5.10, 9.05 meq/100g). This may due to MMT addition increasing 1) the formation of oxygenated fucntional groups and 2) the Lewis acid sites of MMT itself.

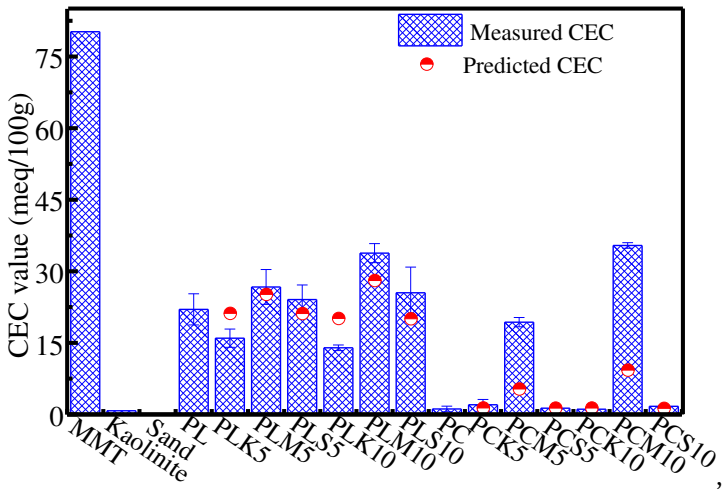

Figure 2. CEC values of prepared biochar

3.1.4 SEM-EDX and XRD

SEM images in Fig.3a show that the surface of composite samples (PCM5) is a layered structure, which is a common clay mineral structure(Yao et al., 2014; Zhou et al., 2009). EDX results (Fig.3b) show high contents of Si, Al, Na, Ca and Mg, further indicating that the composite surface is widely covered by clay minerals, despite their relatively low concentrations. Fig.3c shows the distribution of Ca in the entire EDX test

area, indicating that the MMT particles were successfully loaded onto the biochar. XRD result of PCM5 also indicated the presence of mineral crystals. In the spectrum (Fig.3d), three peaks at 5.4°,19.6° and 35.3°(d=18 Å) were identified as MMT, which was consistent with EDX results.

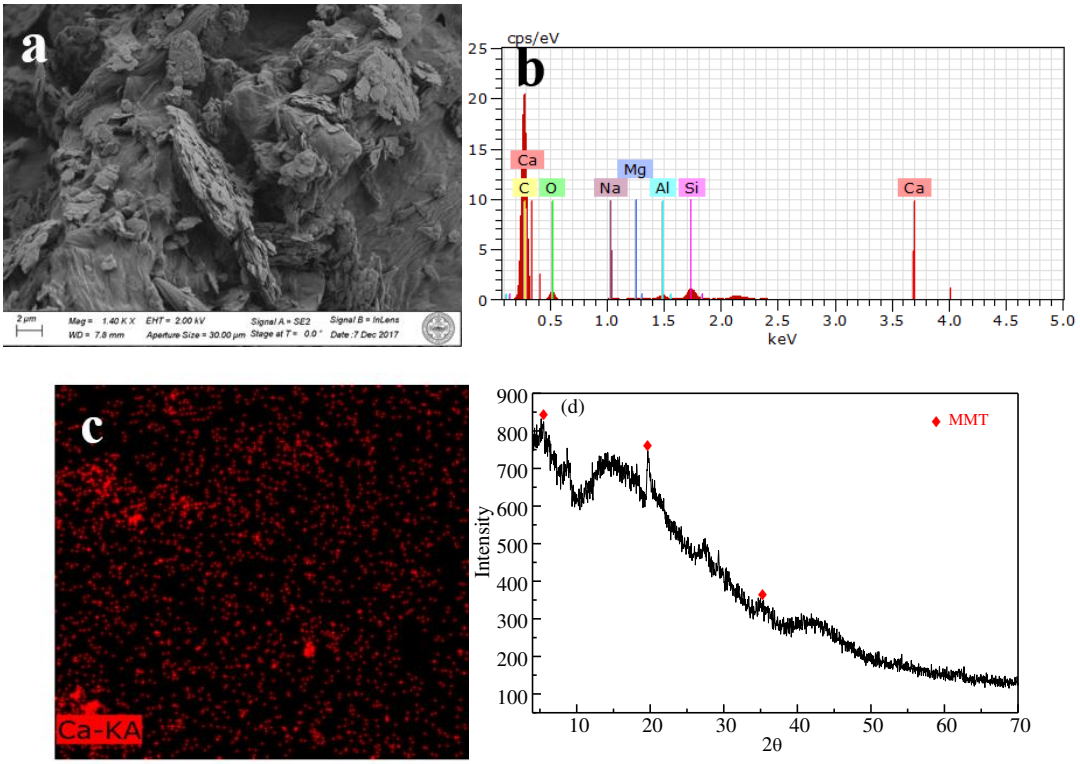

Figure 3. SEM images and XRD spectrum of prepared biochar (Cellulose with 5*wt*% MMT)

3.2 Application of Biochars to Adsorption of Aqueous Contaminants

3.2.1 Equilibrium isotherm study

The biochars with 5*wt*% mineral loading were used to determine the potential for these composite biochars to remove aqueous organic contaminants. The resulting adsorption model parameters of MB onto biochar are presented in Table 2. Equilibrium adsorption studies indicate that the maximum adsorption capacities of the mineral-biochar composites ranging from 11 to 110 $mg_{MB}/g_{biochar}$. Samples closely adhered to Langmuir isotherm as determined through correlation coefficients (R^2>0.99) for each model

(Figure S1 and Table 2), indicating that adsorption of MB is monolayer and thus likely chemical in nature. As shown in Fig. 4(a), the cellulose-based biochars had a greater MB adsorption capacity than the oak leaf biochars. Surface modification with MMT and kaolinite did dramatically improve MB adsorption capacity for cellulose biochars, while it had no obvious effect on the adsorption capacity of leaf-based char, indicating that it may not suitable to apply the leaf-mineral composite for MB removal. For cellulose, the MMT modification improved the MB adsorption capacity from 23.915 mgMB/g to 109.9653 mgMB/g, while 36.444 mgMB/g for kaolinite modification. These results should be associated with the physico-chemical property of adsorbents. Generally, electrostatic attraction was the major adsorption interaction between engineered biochar and cationic dye MB(Wang et al., 2016). In order to verify the charge property of these biochars, zeta potential values in DI water were provided in Table 3. It could be found that all biochars showed negative surface charge, and PC possessing a highest zeta potential among them. Nonetheless, the uptake value of MB in PC was far lower than PCM5, which indicated that electrostatic attraction was not the key factor. Porous structure might facilitate better adsorption due to the favorable mass transportation and more active sites (Ge et al., 2018). Meanwhile, Li and Zhang investigated the influence of porous structure on the adsorption of MB, indicating 3.05 nm (which was the 5 times of MB three-dimensional structure depth) was the separation point (Li and Zhang, 2019). We could observe that cellulose biochar with a larger pore size (3.2-5.8 nm>3.05 nm) exhibited much higher adsorption capacity than leaf-biochar with lower pore size (~2.5 nm). Therefore, the coupling of other physico-chemical

properties of biochar under larger pore size was the key factor for engineered biochar to adsorb MB.

The improvement in adsorption capacity (AC) as a function of clay mineral loading is likely not due to the higher AC contribution of clays alone, whose AC were measured to be 727.76 (MMT) and 18.67 (kaolinite) $mg_{MB}/g_{Adsorbent}$. The biomass: clay mineral ratio was initially 95:5, but the AC of PCM5 and PCK5 increased much higher than 5.26%. If the clay mineral did not interact with biomass to increase the AC of composite, one might expect the resulting PCM5 AC to be ~59 $mg/g_{Adsorbent}$ [if ($AC_{predict}$ = (0.95)($AC_{Cellulose\ biochar}$)+(0.05)($AC_{MMT/Kaolinite}$))], yet the actual AC was almost twice this value. It might be predicted that PCK5 would have an AC of ~23 $mg/g_{Adsorbent}$, yet it was 50% higher than this value. One explanation for the improved AC of composite is that the positive synergistic effect among the composites' physicochemical characterizations, such as surface area, CEC and elemental composition(Brindley and Thompson, 1970; Gürses et al., 2006; Klika et al., 2011).

3.2.2 Adsorption dynamic study

From Table 2 and Figure S4, we can see the adsorption of MB appeared to follow pseudo-second-order kinetics, which further underscores the conclusion that the adsorption of MB to biochar was chemical in nature, likely via electron pair transfer between MB and biochar. Similar results were obtained by Yu *et al* who reported electrons exchange between MB and biochar produced from microalgal was the rate-limiting step(Kai Ling Yu, Xin Jiat Lee, Hwai Chyuan Ong, Wei-Hsin Chen, Jo-Shu Chang, Chih- Sheng Lin, Pau Loke Show, 2020). In addition, we can see that the oak

leaves-based biochar had a faster adsorption rate for MB compared with the cellulose-based biochar, and PCM5's adsorption rate was faster than other cellulose-based char.

In order to understand major limitations in the adsorption process of MB onto mineral-biochar composites, the intra-particle diffusion model was applied to this data. Previous studies have suggested that if q_t vs. $t_{1/2}$ was a straight line and the plot passes through the origin, then intra-particle diffusion is the rate-limiting step in the adsorption process. Otherwise, the adsorption process is controlled by multiple steps(Hameed et al., 2008b; Jang et al., 2018; Kai Ling Yu, Xin Jiat Lee, Hwai Chyuan Ong, Wei-Hsin Chen, Jo-Shu Chang, Chih- Sheng Lin, Pau Loke Show, 2020). As shown in Fig 4(b), the q_t vs. $t_{1/2}$ was fitted by three straight line. The first stage (not shown) was completed within the first 5 min, which is the bulk transport of MB molecules from aqueous solution to the composite's surface. The second and third parts are well represented by straight lines, suggesting that the intraparticle diffusion is the rate-limiting stage. In some cases (with the exception of PCM5 and PLM5), the third straight line was the final equilibrium stage where MB reaches a dynamic equilbrium between the aqueous phase and solid adsorbent. As shown in Fig. 4(b), the drawn straight lines did not pass through the origin and the intercepts might be result from the different mass transfer rate between initial and final of adsorption, indicating other possible mechanisms such as diffusion boundary layer or ion-exchange along with intraparticle diffusion were involved during the adsorption process of MB onto mineral-biochar composites(Kai Ling Yu, Xin Jiat Lee, Hwai Chyuan Ong, Wei-Hsin Chen, Jo-Shu Chang, Chih- Sheng Lin, Pau Loke Show, 2020; Lee et al., 2016).

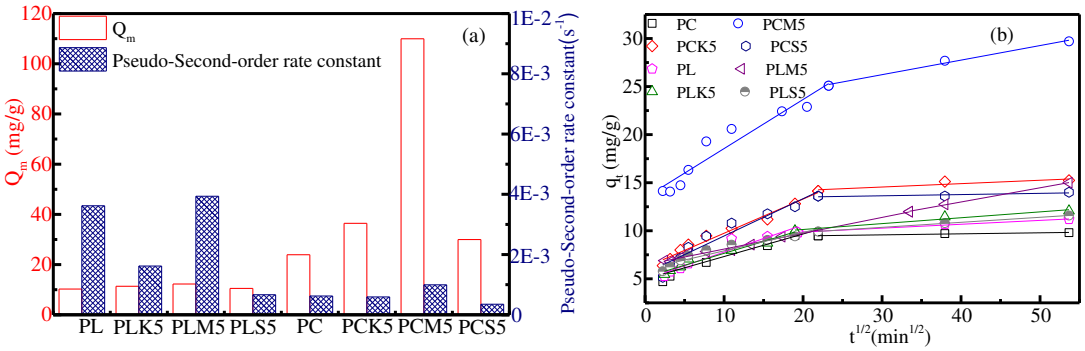

Figure 4. Equilibrium and kinetics adsorption results of MB onto prepared biochar

3.2.3 Comparison with other reported adsorbents

A comparative study was made based on uptake capacity between several bio-char composite adsorbents and the PCM5 for the removal of MB dye. In comparison to other adsorbents, the removal efficiency of the dye was found to be high in PCM5 (Table 4). Hence the PCMS biochar act as a favorable one for MB dyes removal.

359 **Table 2**. Adsorption model parameters of MB onto biochar

Isotherm/Kinetics Model		PL	PLK5	PLM5	PLS5	PC	PCK5	PCM5	PCS5
	K_L (L/mg)	0.603	0.267	0.170	0.170	0.772	0.374	0.3276	0.0512
	Q_m (mg/g)	10.256	11.351	12.270	10.504	23.915	36.444	109.9653	29.9760
Langmuir	R^2	0.993	0.993	0.983	0.988	0.994	1.000	0.9997	0.9966
	K_f (mg/g (L/mg)$^{1/n}$)	5.292	1.607	4.262	1.562	16.423	28.104	3.9700	9.0761
	n	5.790	4.852	4.110	5.160	11.302	19.694	0.5708	4.5641
Freundlich	R^2	0.706	0.894	0.935	0.951	0.378	0.978	0.8533	0.8865
	K_1 (s^{-1})	0.0014	0.0003	0.0009	0.0008	0.0026	0.0015	0.0028	0.0010
Pseudo-first-order kinetic	R^2	0.528	0.799	0.918	0.775	0.746	0.880	0.9464	0.9000
	K_2 (s^{-1})	0.004	0.0019	0.0047	0.0008	0.0007	0.0007	0.0012	0.0004
Pseudo-second-order kinetic	R^2	0.999	0.997	0.995	0.987	0.994	0.997	0.9983	0.9971

360 Table 3. Zeta potential of engineered biochars

Materials	Zeta potential (mV)	Materials	Zeta potential (mV)
PC	-55.1±2.55	PL	-32.71±2.23
PCM5	-26.69±0.96	PLM5	-22.96±3.40
PCK5	-32.96±2.29	PLK5	-32.93±0.71
PCS5	-18.69±0.94	PLS5	-9.01±0.92

361

362

Table 4 Comparison of adsorption capacity of PCM5 with other bio adsorbents

Bio-adsorbents	Adsorption Capacity(mg/g)
Chitosan nanocomposite(Rahmi et al., 2019)	20.49
Coconut bunch waste (Hameed et al., 2008a)	70.92
Kaolin (Mouni et al., 2018)	52.7
Orange peel (Annadurai et al., 2002)	13.9
Tea waste (Uddin et al., 2009)	85.1
MMDM derived biochar (Hoslett et al., 2020)	7.2
Rice husk (Vadivelan and Vasanth Kumar, 2005)	40.59
PCM5 (This work)	109.9

3.2.4 Comparison with other reported adsorbents

The adsorption of MB onto biochar is a complex process, including multiple steps and mechanisms, mainly involving electrostatic interaction, hydrogen bonding, surface complexation, ion exchange and π-π EDA interaction, etc(Alqadami et al., 2018; Liao et al., 2019; Yao et al., 2018). The nature of the adsorbent affects the relative contribution of these various interactions(Liao et al., 2012). Liao *et al*. indicated that surface area, oxygen and hydrogen content, aromatic (H/C) were related to van der waals' force, H-bonding and π-π EDA interaction, respectively(Liao et al., 2012; Pan and Xing, 2008; Wang et al., 2011). To measure the relative magnitude of these interactions, a multiple linear regression model relating adsorption capacity (q_m) and adsorbent physicochemical properties was developed in SPSS software. The conceptual model is expressed as follows:

$$q_m = aA_{surf} + bB_{Pore\ volume} + dD_{Ash} + eE_{H/C} + fF_{O/C} + gG_{CEC} + hH_{O+H} + i \quad \text{Eq.(1)}$$

Where a,b,c,d,e,f,g,h and i represent fitting constants. Both mineral-biochar composite properties of surface area (A_{surf}), pore volume ($B_{Pore\ volume}$), pore size ($C_{Pore\ size}$), ash content (D_{ash}), aromatic ratio of hydrogen to carbon ($E_{H/C}$), polarity ratio of

oxygen to carbon ($F_{O/C}$), cation exchange capacity (G_{CEC}), oxygen and hydrogen content (H_{O+H}) are used to give an overall measurement of the interaction. (Previous studies have shown that surface area and pore volume[37], ash (Liu et al., 2020), elemental content(Chen et al., 2017; Liao et al., 2012; Zhao and Zhou, 2019) and CEC(Chen et al., 2017) are all related to adsorption performance).

$$q_m = 1029.738B_{Pore\ volume} - 14.609D_{Ash} + 1268.744E_{\frac{H/C}{C}} - 159.944F_{\frac{O/C}{C}} + 0.453G_{CEC} + 16.899H_{O+H} - 321.92 \quad \text{Eq.(2)}$$

R^2=0.981，F=4.368，n=8，D-W=2.961

A linear relationship was achieved between q_m and the properties of mineral-char composites, where surface area was removed due to the lower correlation. T-test results (Table 3) indicate that all the explicative variables in Eq.(2) with the exception of ash and adsorbent polarity (O/C) significantly influenced q_m, and the significant degrees follow Pore volume > O+H > H/C> CEC. This indicates that the MB molecule adsorbed onto mineral-biochar composites was the results of the combined effects of surface adsorption, hydrogen bonding, ion exchange and π-πDEA interaction (as shown in Fig.5). and the pore volume effect and hydrogen bonding were the dominated ones.

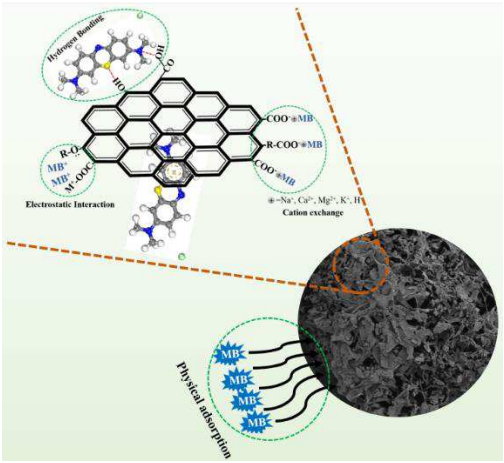

Figure 5 The mechanisms involved in MB adsorption onto mineral-biochar composites

From this multiparameter linear regression model, we see that pore volume and oxygen and hydrogen content were the controlling properties of mineral-biochar composites to adsorb MB. To increase the adsorption capacity of MB, it may be necessary to apply pore reaming and surface modification coupled methods (such as physical activation-steaming exploration(Miao et al., 2019), chemical activation-KOH activation(Qu et al., 2021)) to produce a composite with higher pore volume and increase the oxygen and hydrogen content. Further research will explore the relationship between adsorbent properties and coexistence of multiple pollutants with different nature, then developing and designing the upgraded biochar to removal pollutants with maximum capacity.

Table 3. Coefficients of the multiple linear regression equation

	Unstandardized coefficients		Standardized coefficients		Collinearity statistics	
Explicative variable	B	Beta	*t*	Sig.	Tolerance	VIF[a]
i	-321.923		-2.518	0.241		
Pore volume	1029.738	1.921	4.512	0.139	0.203	4.934
Ash	-14.609	-3.426	-1.41	0.393	0.006	160.69
H/C	1268.744	0.707	1.142	0.458	0.096	10.411
O/C	-159.944	-0.768	-0.388	0.765	0.009	106.697
CEC	0.453	0.147	0.153	0.903	0.04	24.895
O+H	16.899	4.755	1.789	0.325	0.005	192.246

[a] Variance of inflation factor, VIF=1/Tolerance. (VIF>10, indicating that there is a significant multiple linear relationship between variables).

4 Conclusions

A composite mineral-biochar was assembled through the pyrolysis of biomass-mineral blends. Compared with pure biomass char, the sand-char has almost same properties, while the MMT-biochar composites show a strengthening in aromatic structure, and an increase in oxygen-containing surface functional groups and cation

exchange capacity. Composite cellulose-based biochars had a greater adsorption capacity for methylene blue than oak leaves-based biochars, while their adsorption rates were lower than oak leaves chars. The MMT/kaolinite-biochar composite has a higher adsorption capacity for MB than biomass only or biomass-sand-char, and the adsorption capacity of 5wt% MMT loading cellulose char is 5 times higher than pure cellulose char. The adsorption of methylene blue onto the mineral-biochar composites was a result of the synergistic effects of various interactions, as demonstrated via a multiparameter linear regression model. The pore volume effect and hydrogen bonding were the dominant factors controlling the adsorption process. Overall, we find that composite mineral-biochars may be a potential low-cost material with an upgraded adsorption capacity for adsorbing pollutants from wastewater.

Acknowledgements

L.Gao acknowledges the support of the Fundamental Research Funds for the Central Universities (Grant no. 2020QN37) and the support of the China Scholarship Council (CSC) under Grant CSC NO. 201606420017.

Author contributions

Lihui Gao: methodology, materials preparation, origin draft preparation; Jillian Goldfarb: review and editing.

Availability of data and materials: All data generated or analyzed during this study are included in this published article.

Declarations

Ethics approval and consent to participate: Not applicable

Consent for publication: Not applicable

Conflict of interest: The authors declare no competing interests.

References:

Abou-El-Sherbini, K.S., Hassanien, M.M., 2010. Study of organically-modified montmorillonite clay for the removal of copper(II). J. Hazard. Mater. 184, 654–661. https://doi.org/10.1016/j.jhazmat.2010.08.088

Ahmad, M., Lee, S.S., Dou, X., Mohan, D., Sung, J.K., Yang, J.E., Ok, Y.S., 2012. Effects of pyrolysis temperature on soybean stover- and peanut shell-derived biochar properties and TCE adsorption in water. Bioresour. Technol. 118, 536–544. https://doi.org/10.1016/j.biortech.2012.05.042

Alqadami, A.A., Naushad, M., Alothman, Z.A., Ahamad, T., 2018. Adsorptive performance of MOF nanocomposite for methylene blue and malachite green dyes: Kinetics, isotherm and mechanism. J. Environ. Manage. 223, 29–36. https://doi.org/10.1016/j.jenvman.2018.05.090

Annadurai, G., Juang, R.S., Lee, D.J., 2002. Use of cellulose-based wastes for adsorption of dyes from aqueous solutions. J. Hazard. Mater. 92, 263–274. https://doi.org/10.1016/S0304-3894(02)00017-1

Basak, B.B., Saha, A., Sarkar, B., Kumar, B.P., Gajbhiye, N.A., Banerjee, A., 2020. Repurposing distillation waste biomass and low-value mineral resources through biochar-mineral-complex for sustainable production of high-value medicinal plants and soil quality improvement. Sci. Total Environ. 1, 1–10.

Basta, A.H., Fierro, V., El-Saied, H., Celzard, A., 2009. 2-Steps KOH activation of rice straw: An efficient method for preparing high-performance activated carbons. Bioresour. Technol. 100, 3941–3947. https://doi.org/10.1016/j.biortech.2009.02.028

464 Basta, A.H., Fierro, V., Saied, H., Celzard, A., 2011. Effect of deashing rice straws on their derived
465 activated carbons produced by phosphoric acid activation. Biomass and Bioenergy 35, 1954–
466 1959. https://doi.org/10.1016/j.biombioe.2011.01.043
467 Brindley, G.W., Thompson, T.D., 1970. Methylene Blue Absorption by Montmorillonites.
468 Determinations of Surface Areas and Exchange Capacities with Different Initial Cation
469 Saturations (Clay-Organic Studies XIX). Isr. J. Chem. 8, 409–415.
470 https://doi.org/10.1002/ijch.197000047
471 Brunauer, S., Emmett, P.H., Teller, E., 1938. Adsorption of Gases in Multimolecular Layers. J. Am.
472 Chem. Soc. 60, 309–319. https://doi.org/citeulike-article-id:4074706\rdoi: 10.1021/ja01269a023
473 Carrier, M., Hardie, A.G., Uras, Ü., Görgens, J., Knoetze, J., 2012. Production of char from vacuum
474 pyrolysis of South-African sugar cane bagasse and its characterization as activated carbon and
475 biochar. J. Anal. Appl. Pyrolysis 96, 24–32. https://doi.org/10.1016/j.jaap.2012.02.016
476 Chcn, G., Pan, J., Han, B., Yan, H., 1999. Adsorption of methylene blue on montmorillonite. J.
477 Dispers. Sci. Technol. 20, 1179–1187. https://doi.org/10.1080/01932699908943843
478 Chen, L., Chen, X.L., Zhou, C.H., Yang, H.M., Ji, S.F., Tong, D.S., Zhong, Z.K., Yu, W.H., Chu,
479 M.Q., 2017. Environmental-friendly montmorillonite-biochar composites: Facile production and
480 tunable adsorption-release of ammonium and phosphate. J. Clean. Prod. 156, 648–659.
481 https://doi.org/10.1016/j.jclepro.2017.04.050
482 Dehkhoda, A.M., Ellis, N., Gyenge, E., 2016a. Effect of activated biochar porous structure on the
483 capacitive deionization of NaCl and ZnCl2 solutions. Microporous Mesoporous Mater. 224, 217–
484 228. https://doi.org/10.1016/j.micromeso.2015.11.041
485 Dehkhoda, A.M., Gyenge, E., Ellis, N., 2016b. A novel method to tailor the porous structure of KOH-

activated biochar and its application in capacitive deionization and energy storage. Biomass and Bioenergy 87, 107–121. https://doi.org/10.1016/j.biombioe.2016.02.023

Dou, G., Goldfarb, J., 2017. In situ upgrading of pyrolysis biofuels by bentonite clay with simultaneous production of heterogeneous adsorbents for water treatment. Fuel 195, 273–283. https://doi.org/10.1016/j.fuel.2017.01.052

Gao, L., Goldfarb, J.L., 2019. Solid waste to biofuels and heterogeneous sorbents via pyrolysis of wheat straw in the presence of fly ash as an in situ catalyst. J. Anal. Appl. Pyrolysis 137, 96–105. https://doi.org/10.1016/j.jaap.2018.11.014

Goldfarb, J.L., Buessing, L., Gunn, E., Lever, M., Billias, A., Casoliba, E.N., Schievano, A., Adani, F., Buessing, L., Botto, A., Casoliba, E.N., Rossoni, M., Goldfarb, J.L., 2017. Novel Integrated Biorefinery for Olive Mill Waste Management: Utilization of Secondary Waste for Water Treatment. ACS Sustain. Chem. Eng. 5, 876–884. https://doi.org/10.1021/acssuschemeng.6b02202

Gürses, A., Doğar, Ç., Yalçin, M., Açikyildiz, M., Bayrak, R., Karaca, S., 2006. The adsorption kinetics of the cationic dye, methylene blue, onto clay. J. Hazard. Mater. 131, 217–228. https://doi.org/10.1016/j.jhazmat.2005.09.036

Hameed, B.H., Mahmoud, D.K., Ahmad, A.L., 2008a. Equilibrium modeling and kinetic studies on the adsorption of basic dye by a low-cost adsorbent: Coconut (Cocos nucifera) bunch waste. J. Hazard. Mater. 158, 65–72. https://doi.org/10.1016/j.jhazmat.2008.01.034

Hameed, B.H., Tan, I.A.W., Ahmad, A.L., 2008b. Adsorption isotherm, kinetic modeling and mechanism of 2,4,6-trichlorophenol on coconut husk-based activated carbon. Chem. Eng. J. 144, 235–244. https://doi.org/10.1016/j.cej.2008.01.028

508 Hoslett, J., Ghazal, H., Mohamad, N., Jouhara, H., 2020. Removal of methylene blue from aqueous
509 solutions by biochar prepared from the pyrolysis of mixed municipal discarded material. Sci.
510 Total Environ. 714, 136832. https://doi.org/10.1016/j.scitotenv.2020.136832
511 Istan, S., Ceylan, S., Topcu, Y., Hintz, C., Tefft, J., Chellappa, T., Guo, J., Goldfarb, J.L., 2016.
512 Product quality optimization in an integrated biorefinery: Conversion of pistachio nutshell
513 biomass to biofuels and activated biochars via pyrolysis. Energy Convers. Manag. 127, 576–588.
514 https://doi.org/10.1016/j.enconman.2016.09.031
515 Jang, H.M., Yoo, S., Choi, Y.K., Park, S., Kan, E., 2018. Adsorption isotherm, kinetic modeling and
516 mechanism of tetracycline on Pinus taeda-derived activated biochar. Bioresour. Technol. 259,
517 24–31. https://doi.org/10.1016/j.biortech.2018.03.013
518 Jiang, M. qin, Jin, X. ying, Lu, X.Q., Chen, Z. liang, 2010. Adsorption of Pb(II), Cd(II), Ni(II) and
519 Cu(II) onto natural kaolinite clay. Desalination 252, 33–39.
520 https://doi.org/10.1016/j.desal.2009.11.005
521 Kai Ling Yu, Xin Jiat Lee, Hwai Chyuan Ong, Wei-Hsin Chen, Jo-Shu Chang, Chih- Sheng Lin, Pau
522 Loke Show, T.C.L., 2020. Adsorptive removal of cationic methylene blue and anionic Congo red
523 dyes using wet- torrefied microalgal biochar: equilibrium, kinetic and mechanism modeling.
524 Environ. Pollut. 1–12. https://doi.org/10.1016/j.envpol.2020.115986
525 Khawmee, K., Suddhiprakarn, A., Kheoruenromne, I., Singh, B., 2013. Surface charge properties of
526 kaolinite from Thai soils. Geoderma 192, 120–131.
527 https://doi.org/10.1016/j.geoderma.2012.07.010
528 Kimetu, J.M., Hill, J.M., Husein, M., Bergerson, J., Layzell, D.B., 2014. Using activated biochar for
529 greenhouse gas mitigation and industrial water treatment. Mitig. Adapt. Strateg. Glob. Chang. 21,

761–777. https://doi.org/10.1007/s11027-014-9625-9

Klika, Z., Pustková, P., Dudová, M., Čapková, P., Kliková, C., Grygar, T.M., 2011. The adsorption of methylene blue on montmorillonite from acid solutions. Clay Miner. 46, 461–471. https://doi.org/10.1180/claymin.2011.046.3.461

Lee, L.Y., Gan, S., Yin Tan, M.S., Lim, S.S., Lee, X.J., Lam, Y.F., 2016. Effective removal of Acid Blue 113 dye using overripe Cucumis sativus peel as an eco-friendly biosorbent from agricultural residue. J. Clean. Prod. 113, 194–203. https://doi.org/10.1016/j.jclepro.2015.11.016

Liao, P., Yuan, S., Zhang, W., Tong, M., Wang, K., 2012. Mechanistic aspects of nitrogen-heterocyclic compound adsorption on bamboo charcoal. J. Colloid Interface Sci. 382, 74–81. https://doi.org/10.1016/j.jcis.2012.05.052

Liao, Y., Li, L., Fan, S., 2019. Removal behavior and mechanism of methylene blue in aqueous solution by rice straw and rice straw-Fe_3O_4 composite. Acta Sci. Circumstantiae 39, 359–370. https://doi.org/10.13671/j.hjkxxb.2018.0318

Liu, B., Fu, M., Xiang, L., Feng, N., Zhao, H., Li, Y., Cai, Q., Li, H., Mo, C., Wong, M., 2020. Adsorption of microcystin contaminants by biochars derived from contrasting pyrolytic conditions: Characteristics, affecting factors, and mechanisms. Sci. Total Environ. 1–10.

Luo, W., Wan, J., Fan, Z., Hu, Q., Zhou, N., Xia, M., Song, M., Qi, Z., Zhou, Z., 2021. In-situ catalytic pyrolysis of waste tires over clays for high quality pyrolysis products. Int. J. Hydrogen Energy 46, 6937–6944. https://doi.org/10.1016/j.ijhydene.2020.11.170

Miao, Z., Gao, M., Wan, K., Pei, Z., He, Q., Ji, P., Bai, L., 2019. Modification of Zhaotong Lignite by Steam Explosion Treatment: Pore Structure and OXygen-Containing FUnctional Groups. Energy & Fuels 33, 4033–4040.

552 Mouni, L., Belkhiri, L., Bollinger, J.C., Bouzaza, A., Assadi, A., Tirri, A., Dahmoune, F., Madani, K.,
553 Remini, H., 2018. Removal of Methylene Blue from aqueous solutions by adsorption on Kaolin:
554 Kinetic and equilibrium studies. Appl. Clay Sci. 153, 38–45.
555 https://doi.org/10.1016/j.clay.2017.11.034
556 Murray, H.H., 1991. Overview - clay mineral applications. Appl. Clay Sci. 5, 379–395.
557 https://doi.org/10.1016/0169-1317(91)90014-Z
558 Pan, B., Xing, B., 2008. Adsorption mechanisms of organic chemicals on carbon nanotubes. Environ.
559 Sci. Technol. 42, 9005–9013. https://doi.org/10.1021/es801777n
560 Qu, J., Wang, Y., Tian, X., Jiang, Z., Deng, F., Tao, Y., Jiang, Q., Wang, L., Zhang, Y., 2021. KOH-
561 activation porous biochar with high specific surface area for adsorptive removal of
562 chromium(VI) and naphathalene from water:Affecting factors, mechanisms and reusability
563 exploration. J. Hazard. Mater. 401, 1–10.
564 Rahmi, Ismaturrahmi, Mustafa, I., 2019. Methylene blue removal from water using H_2SO_4 crosslinked
565 magnetic chitosan nanocomposite beads. Microchem. J. 144, 397–402.
566 https://doi.org/10.1016/j.microc.2018.09.032
567 Segad, M., Jönsson, B., Åkesson, T., Cabane, B., 2010. Ca/Na montmorillonite: Structure, forces and
568 swelling properties. Langmuir 26, 5782–5790. https://doi.org/10.1021/la9036293
569 Suliman, W., Harsh, J.B., Abu-lail, N.I., Fortuna, A., Dallmeyer, I., Garcia-perez, M., 2016. Influence
570 of feedstock source and pyrolysis temperature on biochar bulk and surface properties. Biomass
571 and Bioenergy 84, 37–48. https://doi.org/10.1016/j.biombioe.2015.11.010
572 Sun, P., Hui, C., Khan, R.A., Du, J., Zhang, Q., Zhao, Y.H., 2015. Efficient removal of crystal violet
573 using Fe_3O_4-coated biochar: The role of the Fe_3O_4 nanoparticles and modeling study their

574 adsorption behavior. Sci. Rep. 5, 1–12. https://doi.org/10.1038/srep12638
575 Tan, X., Liu, Shao-bo, Liu, Y., Gu, Y., Zeng, G., Hu, X., Wang, X., Liu, Shao-heng, Jiang, L., 2017.
576 Biochar as potential sustainable precursors for activated carbon production: Multiple applications
577 in environmental protection and energy storage. Bioresour. Technol. 227, 359–372.
578 https://doi.org/10.1016/j.biortech.2016.12.083
579 Tan, X., Liu, Y., Zeng, G., Wang, X., Hu, X., Gu, Y., Yang, Z., 2015. Application of biochar for the
580 removal of pollutants from aqueous solutions. Chemosphere 125, 70–85.
581 https://doi.org/10.1016/j.chemosphere.2014.12.058
582 Tay, T., Ucar, S., Karagöz, S., 2009. Preparation and characterization of activated carbon from waste
583 biomass. J. Hazard. Mater. 165, 481–485. https://doi.org/10.1016/j.jhazmat.2008.10.011
584 Uchimiya, M., Wartelle, L.H., Klasson, K.T., Fortier, C.A., Lima, I.M., 2011. Influence of pyrolysis
585 temperature on biochar property and function as a heavy metal sorbent in soil. J. Agric. Food
586 Chem. 59, 2501–2510. https://doi.org/10.1021/jf104206c
587 Uddin, M.T., Islam, M.A., Mahmud, S., Rukanuzzaman, M., 2009. Adsorptive removal of methylene
588 blue by tea waste. J. Hazard. Mater. 164, 53–60. https://doi.org/10.1016/j.jhazmat.2008.07.131
589 Vadivelan, V., Vasanth Kumar, K., 2005. Equilibrium, kinetics, mechanism, and process design for the
590 sorption of methylene blue onto rice husk. J. Colloid Interface Sci. 286, 90–100.
591 https://doi.org/10.1016/j.jcis.2005.01.007
592 van Zwieten, L., Kimber, S., Morris, S., Chan, K.Y., Downie, A., Rust, J., Joseph, S., Cowie, A., 2010.
593 Effects of biochar from slow pyrolysis of papermill waste on agronomic performance and soil
594 fertility. Plant Soil 327, 235–246. https://doi.org/10.1007/s11104-009-0050-x
595 Vijayalakshmi, P., Bala, V.S.S., Thiruvengadaravi, K. V., Panneerselvam, P., Palanichamy, M.,

596 Sivanesan, S., 2010. Removal of Acid Violet 17 from Aqueous Solutions by Adsorption onto
597 Activated Carbon Prepared from Pistachio Nut Shell. Sep. Sci. Technol. 46, 155–163.
598 https://doi.org/10.1080/01496395.2010.484006
599 Visa, M., Bogatu, C., Duta, A., 2010. Simultaneous adsorption of dyes and heavy metals from
600 multicomponent solutions using fly ash. Appl. Surf. Sci. 256, 5486–5491.
601 https://doi.org/10.1016/j.apsusc.2009.12.145
602 Wang, X., Shu, L., Wang, Y., Xu, B., Bai, Y., Tao, S., Xing, B., 2011. Sorption of peat humic acids to
603 multi-walled carbon nanotubes. Environ. Sci. Technol. 45, 9276–9283.
604 https://doi.org/10.1021/es202258q
605 Wang, X., Zhang, Y., Luo, W., Elzatahry, A.A., Cheng, X., Alghamdi, A., Abdullah, A.M., Deng, Y.,
606 Zhao, D., 2016. Synthesis of Ordered Mesoporous Silica with Tunable Morphologies and Pore
607 Sizes via a Nonpolar Solvent-Assisted Stöber Method. Chem. Mater. 28, 2356–2362.
608 https://doi.org/10.1021/acs.chemmater.6b00499
609 Wu, H., Lai, C., Zeng, G., Liang, J., Chen, J., Xu, J., Dai, J., Li, X., Liu, J., Chen, M., Lu, L., Hu, L.,
610 Wan, J., 2017. The interactions of composting and biochar and their implications for soil
611 amendment and pollution remediation: a review. Crit. Rev. Biotechnol. 37, 754–764.
612 https://doi.org/10.1080/07388551.2016.1232696
613 Yang, B., Cai, Z., Zhao, W., 2009. Catalysis of Different Clay Minerals to Kerabitumen in
614 Hydrocarbon Genesis. Ed. Nat. Sci. 11, 68–71.
615 https://doi.org/10.19406/j.cnki.cqkjxyxbzkb.2009.01.021
616 Yao, S., Zhang, M., Li, L., Liao, Y., Zhou, N., Fan, S., Tang, J., 2018. Preparation of tea waste-nano
617 Fe_3O_4 composite and its removal mechanism of methylene blue from aqueous solution. Environ.

618 Chem. 37, 96–107.
619 Yao, Y., Gao, B., Fang, J., Zhang, M., Chen, H., Zhou, Y., Creamer, A.E., Sun, Y., Yang, L., 2014.
620 Characterization and environmental applications of clay-biochar composites. Chem. Eng. J. 242,
621 136–143. https://doi.org/10.1016/j.cej.2013.12.062
622 Zhang, M., Gao, B., 2013. Removal of arsenic , methylene blue , and phosphate by biochar/AlOOH
623 nanocomposite. Chem. Eng. J. 226, 286–292. https://doi.org/10.1016/j.cej.2013.04.077
624 Zhang, M., Gao, B., Varnoosfaderani, S., Hebard, A., Yao, Y., Inyang, M., 2013. Preparation and
625 characterization of a novel magnetic biochar for arsenic removal. Bioresour. Technol. 130, 457–
626 462. https://doi.org/10.1016/j.biortech.2012.11.132
627 Zhao, Z., Zhou, W., 2019. Insight into interaction between biochar and soil minerals in changing
628 biochar properties and adsorption capacities for sulfamethoxazole. Environ. Pollut. 245, 208–
629 217.
630 Zhou, L., Chen, H., Jiang, X., Lu, F., Zhou, Y., Yin, W., Ji, X., 2009. Modification of montmorillonite
631 surfaces using a novel class of cationic gemini surfactants. J. Colloid Interface Sci. 332, 16.21.
632

Figures

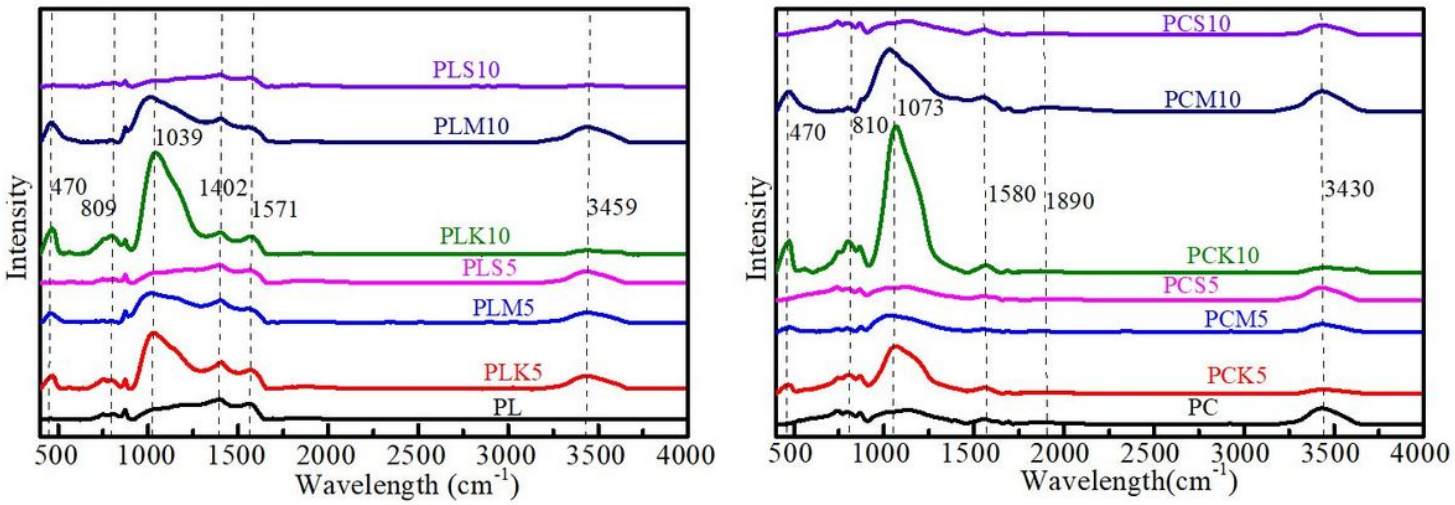

Figure 1

FTIR spectra of prepared biochar

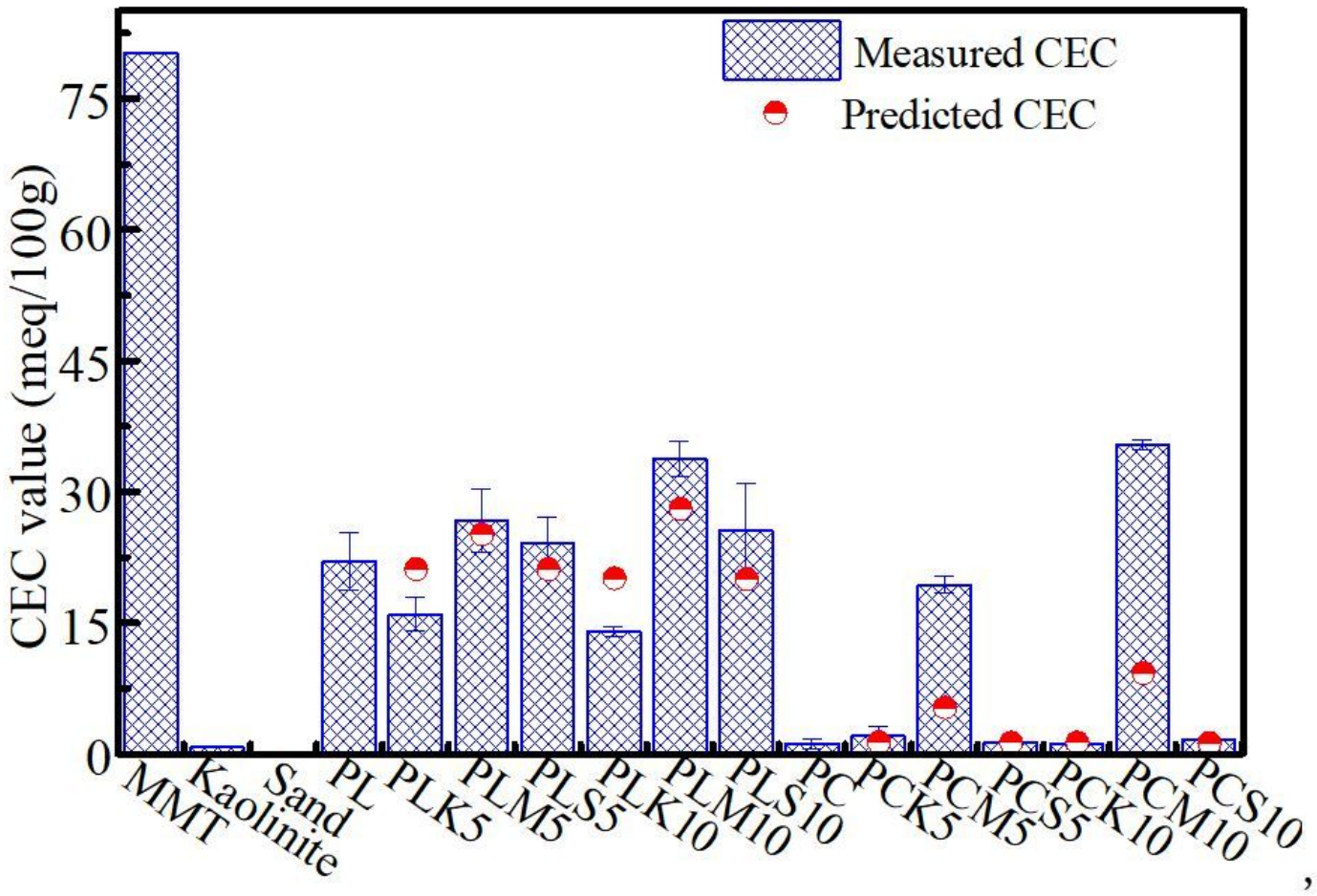

Figure 2

CEC values of prepared biochar

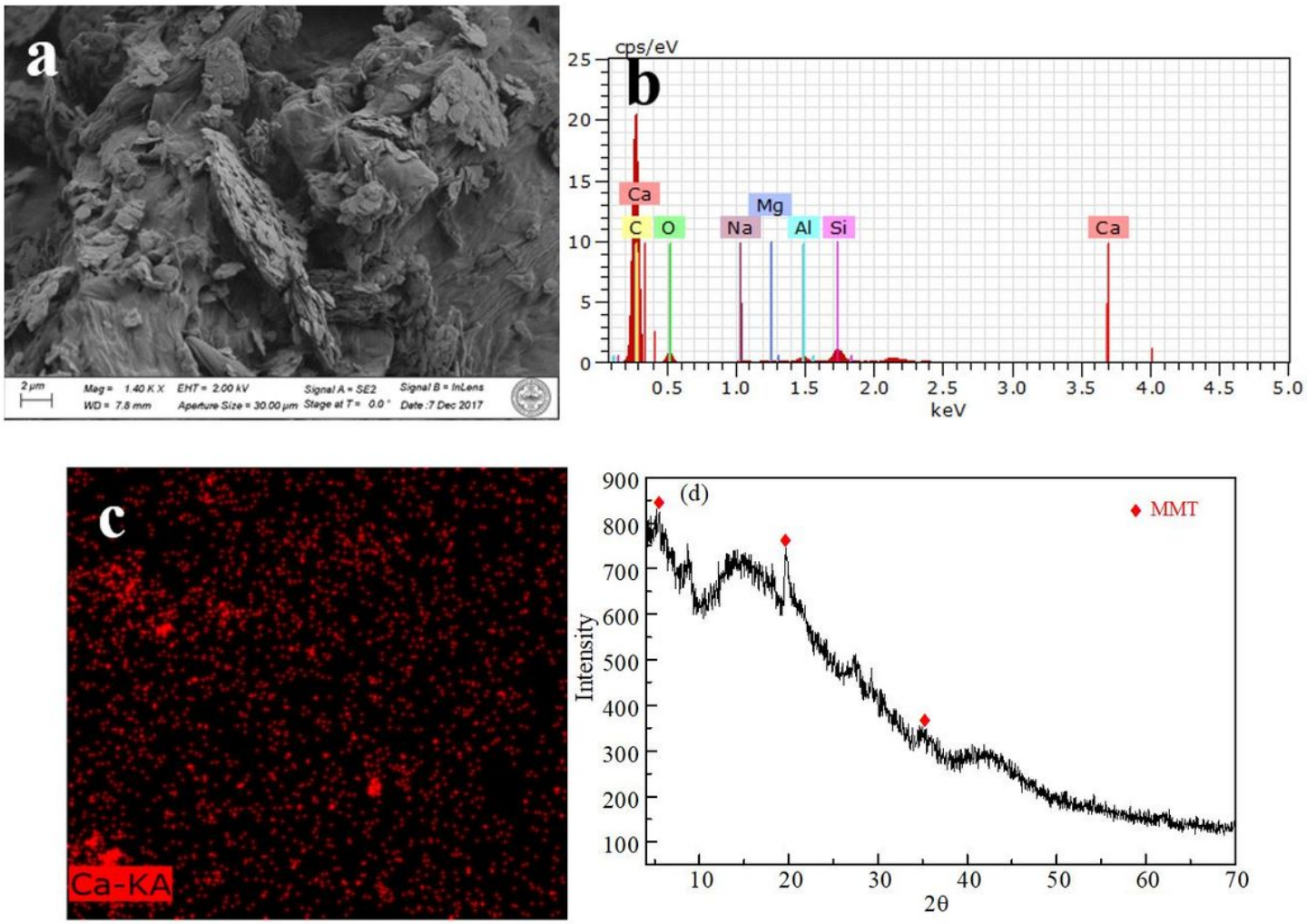

Figure 3

SEM images and XRD spectrum of prepared biochar (Cellulose with 5wt% MMT)

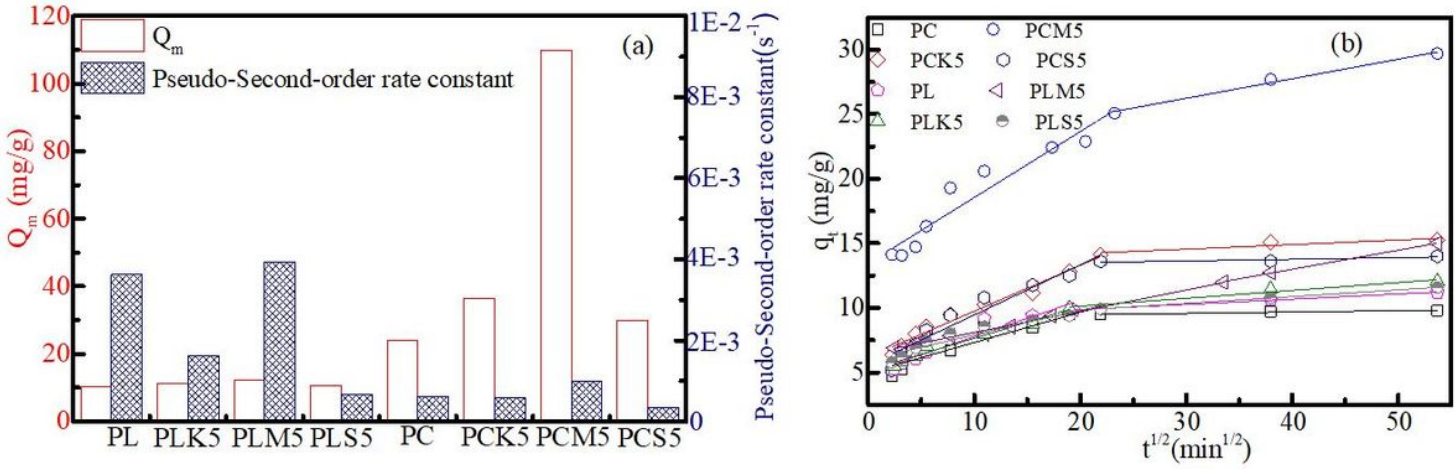

Figure 4

Equilibrium and kinetics adsorption results of MB onto prepared biochar

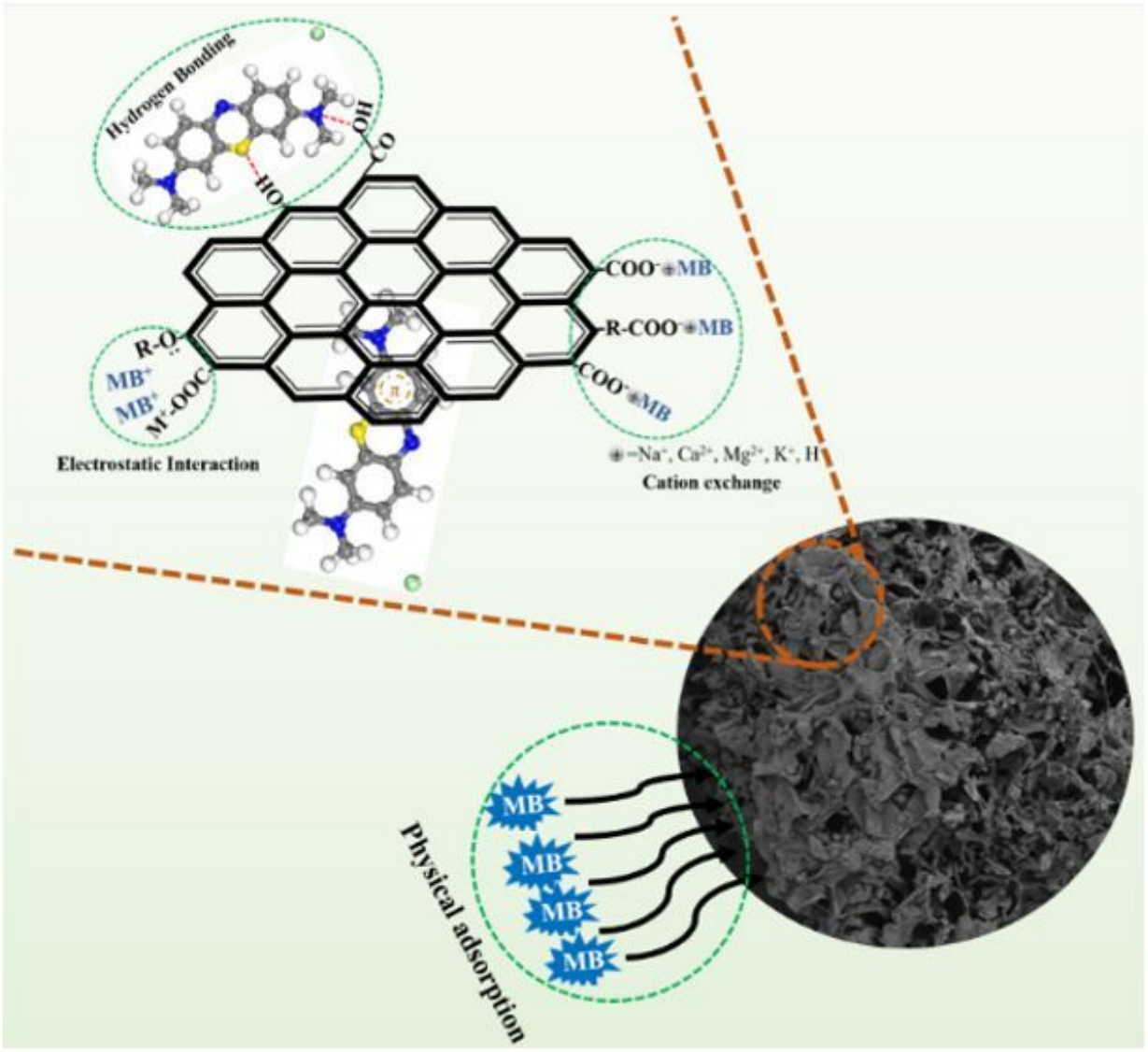

Figure 5

The mechanisms involved in MB adsorption onto mineral-biochar composites